

## Article

# Optical, Dielectric, and Electrical Properties of Tungsten-Based Materials with the Formula $\text{Li}_{(2-x)}\text{Na}_x\text{WO}_4$ ( $x = 0, 0.5, \text{ and } 1.5$ )

Moufida Krimi <sup>1</sup>, Mohammed H. Al-Harbi <sup>2</sup>, Abdulelah H. Alsulami <sup>3</sup>, Karim Karoui <sup>1</sup>, Mohamed Khitouni <sup>4,\*</sup> and Abdallah Ben Rhaïem <sup>1</sup> 

<sup>1</sup> Laboratory LaSCOM, Faculty of Sciences of Sfax, University of Sfax, BP1171, Sfax 3000, Tunisia; krimi.fayda@gmail.com (M.K.); karouikarim36@yahoo.com (K.K.); abdallahrhaïem@yahoo.fr (A.B.R.)

<sup>2</sup> Department of Science, King Abdulaziz Military Academy, Riyadh 11538, Saudi Arabia

<sup>3</sup> Chemistry Department, Faculty of Science and Arts in Baljurashi, Al-Baha University, Al-Baha 65431, Saudi Arabia; aalsulami@bu.edu.sa

<sup>4</sup> Department of Chemistry, College of Science, Qassim University, Buraidah 51452, Saudi Arabia

\* Correspondence: kh.mohamed@qu.edu.sa

**Abstract:** In the present study, three chemical compounds,  $\text{Li}_2\text{WO}_4$ ,  $\text{Li}_{0.5}\text{Na}_{1.5}\text{WO}_4$ , and  $\text{Li}_{1.5}\text{Na}_{0.5}\text{WO}_4$ , are produced using the solid–solid method. Unlike the compound  $\text{Li}_{0.5}\text{Na}_{1.5}\text{WO}_4$ , which crystallizes in the orthorhombic system with the space group Pmmm, both compounds  $\text{Li}_2\text{WO}_4$  and  $\text{Li}_{1.5}\text{Na}_{0.5}\text{WO}_4$  crystallize in the monoclinic system with the space group P2/m. A morphological analysis reveals that all three compounds have a compact structure with some porosity present. An EDX analysis confirms the chemical composition of the three samples. The optical measurements provide information on the optical gaps and Urbach energies of the materials under consideration. Their dielectric characteristics are investigated in a frequency range of 100–106 Hz and at temperatures ranging from 300 to 600 K. Moreover, this research enables us to determine the ferroelectric transition as well as the type of dielectric material. In this study, an investigation of electrical conductivity was conducted for well-defined temperature and frequency values; which provided us with information about the mechanism of conduction and charge carrier transport models.



**Citation:** Krimi, M.; Al-Harbi, M.H.; Alsulami, A.H.; Karoui, K.; Khitouni, M.; Ben Rhaïem, A. Optical, Dielectric, and Electrical Properties of Tungsten-Based Materials with the Formula  $\text{Li}_{(2-x)}\text{Na}_x\text{WO}_4$  ( $x = 0, 0.5, \text{ and } 1.5$ ). *Crystals* **2023**, *13*, 1649.

<https://doi.org/10.3390/cryst13121649>

Academic Editor: Andrey Prokofiev

Received: 7 October 2023

Revised: 15 November 2023

Accepted: 18 November 2023

Published: 30 November 2023



**Copyright:** © 2023 by the authors. Licensee MDPI, Basel, Switzerland. This article is an open access article distributed under the terms and conditions of the Creative Commons Attribution (CC BY) license (<https://creativecommons.org/licenses/by/4.0/>).

**Keywords:** tungsten-based materials; physical chemistry; optical properties; electrical conductivity; mechanism of conduction

## 1. Introduction

In an effort to find new materials with a wide range of commercial uses, several ceramics, single crystals, and thin films of various structural families have been synthesized and described during the past few years, utilizing a variety of experimental techniques [1–24]. In this regard, research projects carried out in the last several years have shown a great deal of interest in tungsten-based materials [3–6]. There is constant innovation in this subject because tungsten has so many attractive characteristics. In fact, the use of tungsten-based materials is popular in a variety of fields, including photoluminescence [1,2], magnetic characteristics [3], supercapacitors [4,5], laser hosts [6,7], gas sensing [8,9], catalysts [10,11], photocatalysts [12–14], scintillator materials [15,16], humidity sensors [17,18], microwave applications [19,20], fiber optics [21,22], lithium batteries [23,24], etc. Because of their high specific capacity, good operating voltage, large reserves, and environmental friendliness, these materials have proven beneficial for electrochemical energy storage. With a melting temperature of roughly 3380 °C and a boiling point of roughly 5900 °C, tungsten is a thermally stable substance. Furthermore, because of its excellent coloration efficiency, strong reversibility ratio, rapid colorization bleaching speed, and lengthy cyclic stability, it is recyclable and not considered a health hazard [25,26]. These characteristics help explain tungsten’s remarkable success in a variety of applications. In fact, the literature mentions a number of tungsten-based compounds such as  $\text{ABWO}_4$  and  $\text{A}_2\text{WO}_4$  ( $A, B = \text{Li, Na, K,}$

etc.), which were discovered to have a variety of structures [27,28], substantial phase transitions [29,30], and considerable electrical [31,32] and ferroelectric properties [33].  $\text{Li}_2\text{WO}_4$  and  $\text{Na}_2\text{WO}_4$  compounds, for instance, have been the topic of numerous prior investigations employing various techniques of production. Both compounds show a ferroelectric transition, at  $T_c = 278$  K for  $\text{Li}_2\text{WO}_4$  and at  $T_c = 300$  K for  $\text{Na}_2\text{WO}_4$  [5,6]. Ferroelectric and ferroelastic transitions are mainly found in tungsten forms containing either a monovalent element alone or a monovalent element coupled with a bivalent element. Moreover, the samples containing mainly bivalent elements are unlikely to exhibit ferroelectric transitions. The XRD, EDF, and SEM analyses of  $\text{Li}_{2-x}\text{Na}_x\text{WO}_4$  ( $x = 0, 0.5$ , and  $1.5$ ), which have been realized and published by Krimi et al. confirm the purity and the stoichiometry of these materials [6,34,35]. The samples  $\text{Li}_2\text{WO}_4$  and  $\text{Li}_{1.5}\text{Na}_{0.5}\text{WO}_4$  crystallize in the monoclinic system (space group:  $P2_1/m$ ), while the other compounds,  $\text{Na}_2\text{WO}_4$  and  $\text{Li}_{0.5}\text{Na}_{1.5}\text{WO}_4$ , crystallize in the orthorhombic system (space groups:  $Pbca$  for  $\text{Na}_2\text{WO}_4$  and  $Pmmm$  for  $\text{Li}_{0.5}\text{Na}_{1.5}\text{WO}_4$ ) [6,34,35]. In fact, a simple comparison of the obtained results leads us to the conclusion that a rise in the sodium rate is accompanied by an increase in the volume of the unit cell, which is expected given that the radius of the sodium atom is larger than that of the lithium atom.

The purpose of the present research is to examine the thermal, optical, and electrical characteristics of the compound  $\text{Li}_{2-x}\text{Na}_x\text{WO}_4$ , as well as the effect of substituting lithium for sodium. Such findings are evaluated in light of the parent chemicals' characteristics.

## 2. Materials and Methods

### 2.1. Synthesis

The solid–solid method was used to synthesize three compounds:  $\text{Li}_2\text{WO}_4$ ,  $\text{Li}_{0.5}\text{Na}_{1.5}\text{WO}_4$ , and  $\text{Li}_{1.5}\text{Na}_{0.5}\text{WO}_4$ . For this, well-calculated stoichiometric quantities of the precursors  $\text{Li}_2\text{CO}_3$ ,  $\text{Na}_2\text{CO}_3$ , and  $\text{WO}_3$  were mixed and then pulverized. They were initially annealed at 723 K to ensure the discharge of undesired chemicals, particularly carbon. They were then ground again, pelletized, and reheated at 823 K to ensure the compactness of the precursors and reduce the size of the grains.

### 2.2. Equipment

The purity of the samples was determined using the X-ray diffraction powder “Siemens D5000” with  $\text{CuK}\alpha$  radiation ( $\lambda = 1.5406$  Å). The powder morphology was examined using scanning electron microscopy (SEM) in secondary-electron mode at a voltage of 15 kV, the microscope used was the DSM960A ZEISS type (Zeiss, Oberkochen, Germany). The SEM was coupled with a Vega&Tescan energy dispersive X-ray spectrometry (EDS) analyzer (Zeiss, Oberkochen, Germany).

To determine the optical band gap and Urbach energy, a UV-Vis measurement was made at room temperature using a spectrophotometer (Shimadzu, Kyoto, Japan, UV-3101PC), while an electric measurement was carried out as a function of frequency in the 10–160 kHz range at temperatures ranging from 458 K to 623 K using a TEGAM 3550 impedance analyzer driven by a microcomputer.

The phase transition in different samples was first detected using a calorimetric study. This was later carried out in a Mettler–Toledo DSC822 apparatus under an Argon atmosphere, at temperatures ranging from 300 to 450 K and at a heating rate of 10 K/min. The annealing of different samples was also performed in the DSC under a 20 mL/min Ar flow.

## 3. Results

### 3.1. Structural and Morphological Studies

Figure 1 depicts the XRD patterns of the synthesized compounds:  $\text{Li}_{0.5}\text{Na}_{1.5}\text{WO}_4$ ,  $\text{Li}_{1.5}\text{Na}_{0.5}\text{WO}_4$ , and  $\text{Li}_2\text{WO}_4$ . Each diffractogram shows the following: the experimental points (black circles), the calculated curve (red line), the difference between the experimental and calculated profiles (blue line), and the Bragg positions (green line). We have been careful to follow the known sequence of steps in order to release different crystallographic

parameters during the structural refining process of the three samples [36]. This confirms the refinement's stability when all the parameters become available. As shown, there is a good level of agreement between the calculated and experimental diagrams. The structural study demonstrates that the compound  $\text{Li}_{0.5}\text{Na}_{1.5}\text{WO}_4$  crystallizes in the orthorhombic system with the space group Pmmm ( $a = 22.42 \text{ \AA}$ ,  $b = 15.21 \text{ \AA}$ ,  $c = 7.18 \text{ \AA}$ ) [35]. As long as the compounds  $\text{Li}_{1.5}\text{Na}_{0.5}\text{WO}_4$  and  $\text{Li}_2\text{WO}_4$  crystallize in the monoclinic system with the space group P2/m, the lattice parameters of the compound  $\text{Li}_{1.5}\text{Na}_{0.5}\text{WO}_4$  are as follows:  $a = 15.92 \text{ \AA}$ ,  $b = 7.19 \text{ \AA}$ ,  $c = 7.18 \text{ \AA}$ ,  $\alpha = \gamma = 90^\circ$ , and  $\beta = 114.31^\circ$ , while those of the compound  $\text{Li}_2\text{WO}_4$  are  $a = 7.49 \text{ \AA}$ ,  $b = 8.31 \text{ \AA}$ ,  $c = 5.92 \text{ \AA}$ ,  $\alpha = \gamma = 90^\circ$ , and  $\beta = 96.81^\circ$  [6,34]. It may be observed that the volume of the elementary unit of the crystal lattice increases as the Na proportion rises.

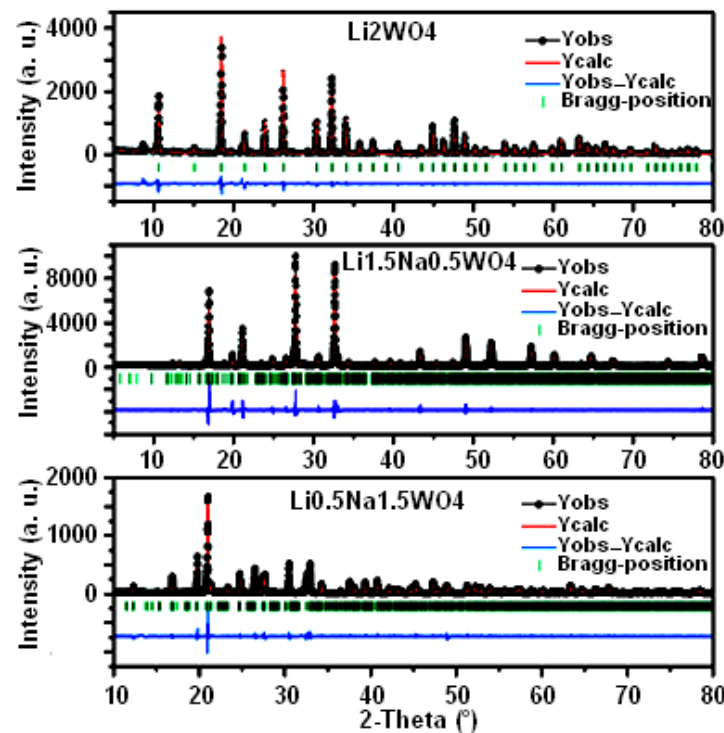


**Figure 1.** XRD patterns and Rietveld refinements for samples of  $\text{Li}_{0.5}\text{Na}_{1.5}\text{WO}_4$ ,  $\text{Li}_{1.5}\text{Na}_{0.5}\text{WO}_4$ , and  $\text{Li}_2\text{WO}_4$  [6,34,35].

On the other hand, several methods have been developed to separate the microstructural parameters including the Williamson–Hall [37] and Halder–Wagner [38] methods. Crystallite size and lattice distortions yield to line broadening. Thus, the total line broadening  $\beta$  can be expressed as [39]

$$\beta = \frac{k\lambda}{D} \frac{1}{\cos\theta} + 4\epsilon \tan\theta \quad (1)$$

where  $D$  is the crystallite size and  $\epsilon$  is the lattice strain. The first term in the right-hand part of Equation (1) is the size contribution and the second term is the lattice distortion. If the peak broadening is due solely to a finite crystallite size, it is assumed that  $\beta = k\lambda / (\langle D \rangle \cos\theta)$ , where  $k$  is close to 1 [40]; this is known as the Scherrer equation [41].

Using the model of Equation (1), the average crystallite size for each studied sample was determined in the current study. This model contains a distinct component for predicting peak broadening related to the crystallite microstrain and uses diffraction peak broadening from at least four diffraction peaks as a foundation for calculating the crystallite size. Equation (1) is a linear equation that considers the isotropic character of the crystals. The inverse of the average crystallite size  $\langle D \rangle$  can be found from the intercept, and the

lattice microstrain ( $\epsilon$ ) can be found from the slope straight line of the plot made with  $(4 \cdot \sin\theta)$  along the  $x$ -axis and  $(\beta \cdot \cos\theta)$  along the  $y$ -axis for the three samples. The average particle sizes for  $\text{Li}_{0.5}\text{Na}_{1.5}\text{WO}_4$ ,  $\text{Li}_{1.5}\text{Na}_{0.5}\text{WO}_4$ , and  $\text{Li}_2\text{WO}_4$  samples were found to be approximately 200, 150, and 100 nm, respectively. The size of a crystallite, which is not always the same as the particle size, is thought to be the size of a coherently diffracting domain. The samples  $\text{Li}_{0.5}\text{Na}_{1.5}\text{WO}_4$ ,  $\text{Li}_{1.5}\text{Na}_{0.5}\text{WO}_4$ , and  $\text{Li}_2\text{WO}_4$  are expected to have lattice strain values of approximately 0.017, 0.035, and 0.043%, respectively. The lattice contraction or expansion in the crystallites, which is the source of the lattice microstrain, is mostly caused by the arrangement of atoms within the crystal lattice. On the other hand, many structural defects (point defects like vacancies, stacking faults, grain boundaries, etc.) are also created in the lattice structure as a result of size refinement and internal–external stresses that result in lattice strain [42,43]. The theoretical estimations of crystallite size derived from the Rietveld refinement for the samples  $\text{Li}_{0.5}\text{Na}_{1.5}\text{WO}_4$ ,  $\text{Li}_{1.5}\text{Na}_{0.5}\text{WO}_4$ , and  $\text{Li}_2\text{WO}_4$  were roughly 27% less than the estimated average crystallite size for the three samples.

Figure 2 gives the SEM images, with resolutions of 9  $\mu\text{m}$  and 40  $\mu\text{m}$ , and the EDX spectra of the three studied compounds. We were able to verify the presence of Na, O, and W elements, as indicated in the EDX spectra. Lithium is the only component that is lacking, and this is because of its low  $Z = 1$  value, which prevents it from emitting X-ray radiation. The SEM images clearly show that the three compounds have a compact structure with just a few pores and a tendency for clustering together because of the humid environment that lithium creates. Also, these images demonstrate a homogeneous distribution of grains with sizes around 5 [36], 2.6, and 4  $\mu\text{m}$  [35] for the three compositions  $\text{Li}_{0.5}\text{Na}_{1.5}\text{WO}_4$ ,  $\text{Li}_{1.5}\text{Na}_{0.5}\text{WO}_4$ , and  $\text{Li}_2\text{WO}_4$ , respectively.

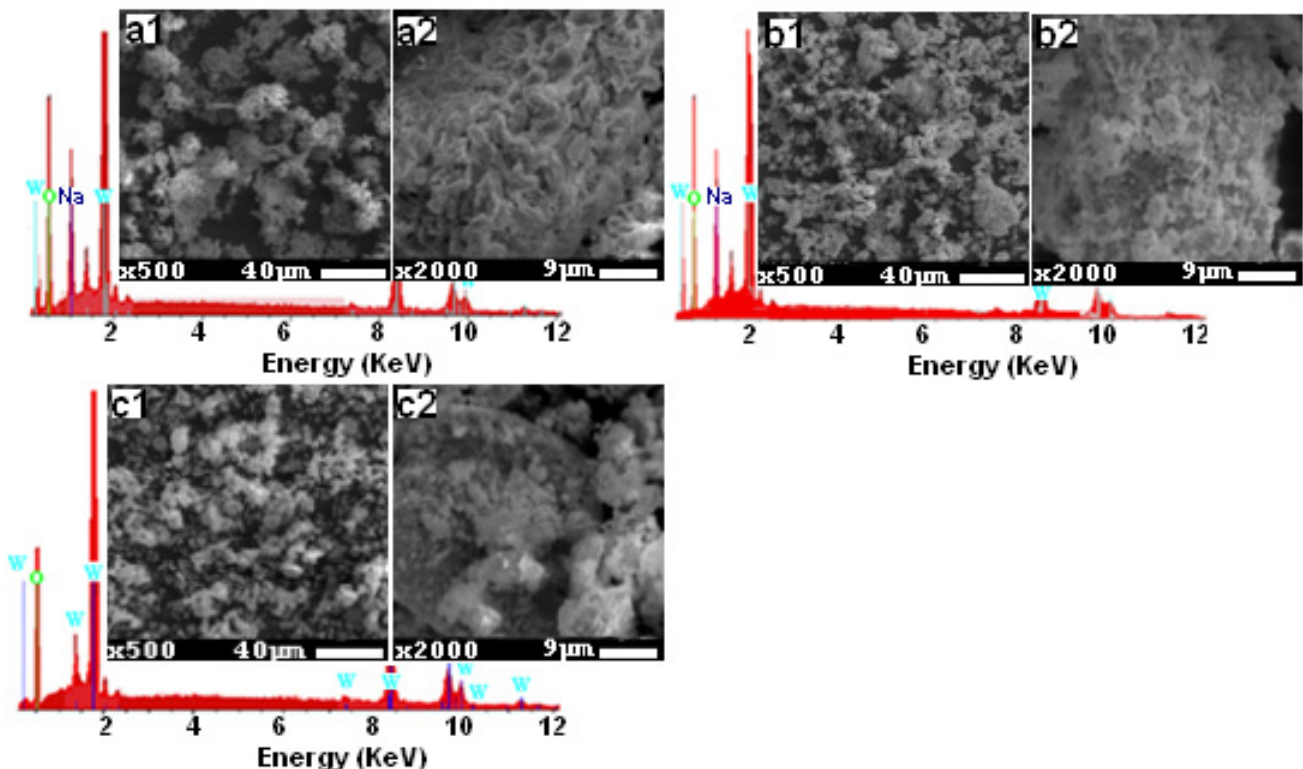


**Figure 2.** SEM micrographs for the studied samples: (a1,a2)  $\text{Li}_{0.5}\text{Na}_{1.5}\text{WO}_4$ , (b1,b2)  $\text{Li}_{1.5}\text{Na}_{0.5}\text{WO}_4$ , and (c1,c2)  $\text{Li}_2\text{WO}_4$ , and the corresponding EDX spectra.

### 3.2. Optical Characterization

Considering the significance of optical characteristics in establishing light efficiency, the gap energy was examined using UV-Vis spectroscopy. The gap energy ( $E_g$ ) is a crucial parameter for the description of materials in the solid state because it links disordered

materials to either a direct or indirect transition through an optical forbidden band and the absorption coefficient ( $\alpha$ ). It takes note of the presence of broad bands rather than peaks in the spectrum. This demonstrates that these molecules contain energetically realized transitions. The investigation of such a spectrum leads to the calculation of the greatest absorption, and thus, based on the literature, the attribution of these bands can be determined. In the spectra presented in Figure 3, one can observe a broad band around 244 nm for the molecule  $\text{Li}_2\text{WO}_4$  and a broad band around 246 nm for the complex  $\text{Li}_{1.5}\text{Na}_{0.5}\text{WO}_4$ . These bands are attributed to the electronic transition from the 2p state of oxygen to the 5d state of tungsten in the  $(\text{WO})^{-2}$  group [8]. The compound  $\text{Li}_{0.5}\text{Na}_{1.5}\text{WO}_4$  shows a similar transition at a wavelength of roughly 300 nm. It can be seen that the structural change reported for this molecule may be the cause of the wavelength change. Indeed, a change in symmetry (from monoclinic to orthorhombic) results in a shift in the atoms' locations and sites.

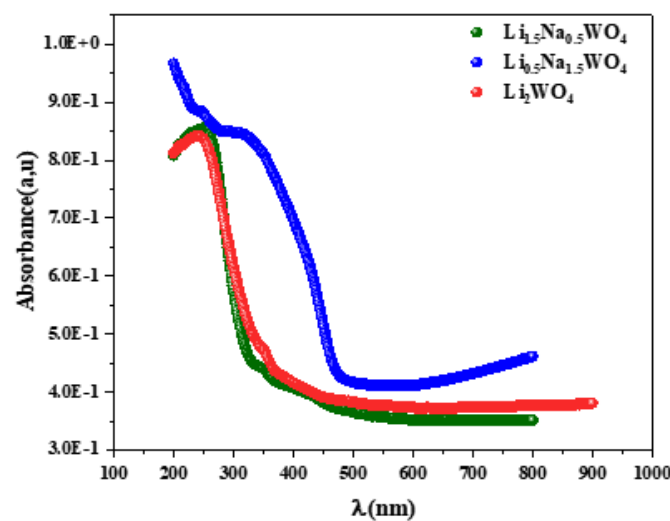


**Figure 3.** Absorbance spectra for the studied compounds.

The Kubelka–Munk method is used to calculate the  $E_g$  on the basis of Equation (1) [44,45]:

$$\frac{F(R)}{e} = \frac{(1 - R)^2}{2R} \quad (2)$$

where  $e$  is the compound's thickness ( $e = 1$  mm),  $R$  is its reflectance, and  $(F(R))/e$  is proportional to the absorption coefficient ( $\alpha$ ). Thus, a modified Kubelka–Munk equation was employed to determine the  $E_g$  by multiplying  $F(R)$  by  $h\nu$  and applying the corresponding coefficient ( $n$ ), which is linked to an electronic transition, as shown by [46]

$$\left( \frac{F(R)}{e} h\nu \right)^n = f(h\nu) \quad (3)$$

in which  $n = 1/2$  represents a direct permitted transition (plotted as  $\alpha(h\nu)^2$  versus  $E$ ) and  $n = 2$  represents an indirect permitted transition (plotted as  $\alpha(h\nu)^{1/2}$  versus  $E$ ).

For our compound, the  $E_g$  was calculated for both types of transitions (Figure 4). To determine the band gap (shown by the red line), we actually extrapolate the curves in the linear section to zero. The band gap values for both the directly permitted transition and the indirectly permitted transition are shown in Table 1. These values clearly show that increased Li levels are associated with rising direct and indirect  $E_g$ , given the variations in the absorption band wavelength and symmetry.

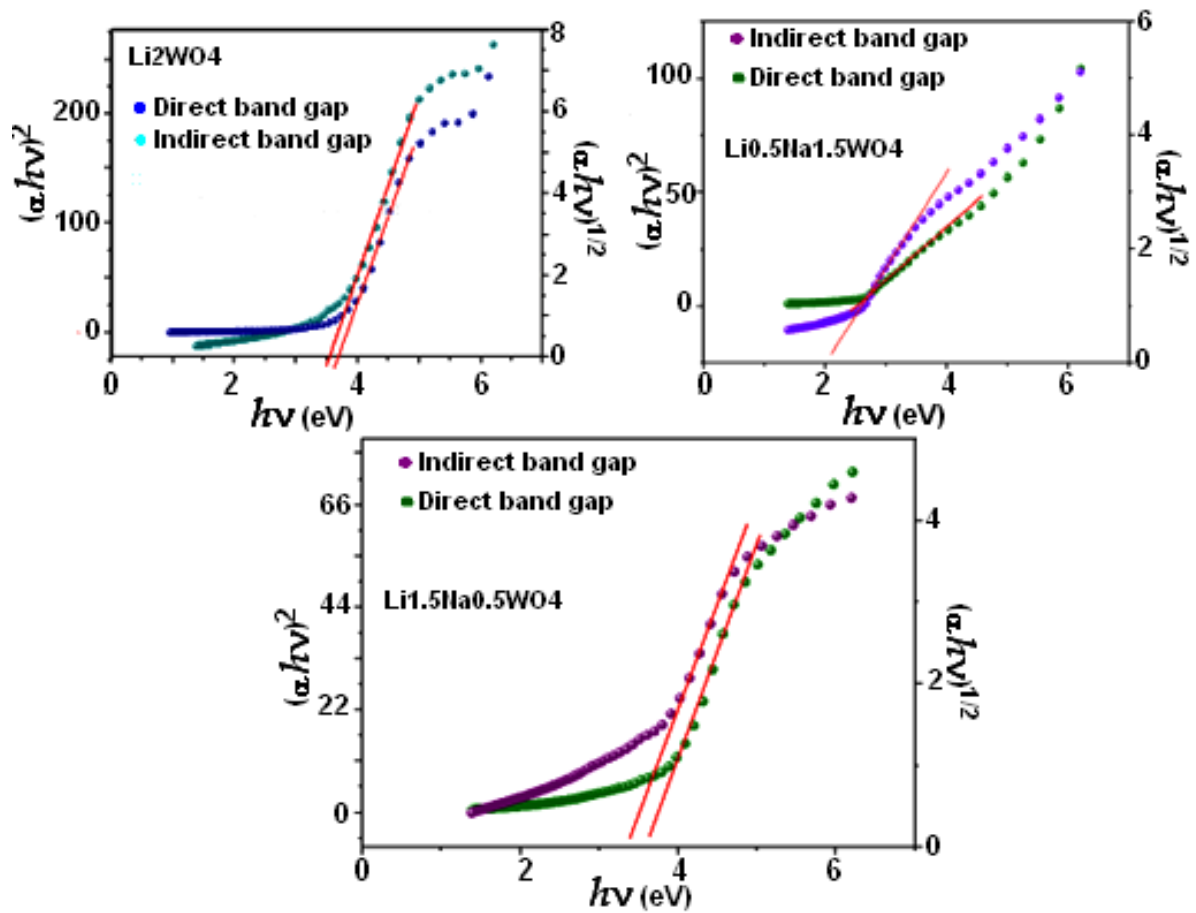


Figure 4. Direct and indirect band gaps for the studied compounds.

Table 1. Calculated values of gap energies for the studied compounds.

Sample	Direct Gap (eV)	Indirect Gap (eV)
Li <sub>2</sub> WO <sub>4</sub>	4.1	3.5
Li <sub>1.5</sub> Na <sub>0.5</sub> WO <sub>4</sub>	3.71	3.4
Li <sub>0.5</sub> Na <sub>1.5</sub> WO <sub>4</sub>	2.6	2.1

Thus, in order to further investigate this pattern, we computed the Urbach Eu energy, which is associated with the changes from the valence band's stretched states to the conduction band's restricted states. On the other hand, the Urbach Eu energy causes the formation of localized states at the tail of the band, near the forbidden band's limits, bounded by the valence and conduction bands. It also describes the compound's disorder [47]. Then, the following empirical formula [46] expresses the relationship between the Urbach energy and the disorder:

$$\alpha = \alpha_0 e^{\frac{h\nu}{E_u}} \quad (4)$$

Furthermore, when plotting the variation in  $\ln(\alpha)$  as a function of energy ( $h\nu$ ), we notice that the following expression governs this curve:

$$\ln(\alpha) = \ln(\alpha_0) + \frac{h\nu}{E_u} \quad (5)$$

where  $\alpha_0$  is a constant and  $E_u$  is the Urbach energy, which is equal to 0.9 eV, 1.36 eV, and 0.35 eV for the Li<sub>2</sub>WO<sub>4</sub>, Li<sub>1.5</sub>Na<sub>0.5</sub>WO<sub>4</sub>, and Li<sub>0.5</sub>Na<sub>1.5</sub>WO<sub>4</sub> compounds, respectively. In fact, as shown in Figure 5, these values are actually determined by taking the inverse of the

curves' slopes. Then, Table 2 shows the computed Urbach energy values. Therefore, based on the above-mentioned results, we can conclude that the compound  $\text{Li}_{1.5}\text{Na}_{0.5}\text{WO}_4$  is the most disordered of the tested compounds. Moreover, an examination of the values of the Urbach energy in relation to the gap one revealed the existence of a harmony in variation, which indicates that the larger the disorder, the wider the gap will be. This suggests that the latter is affected by disorder in our materials.

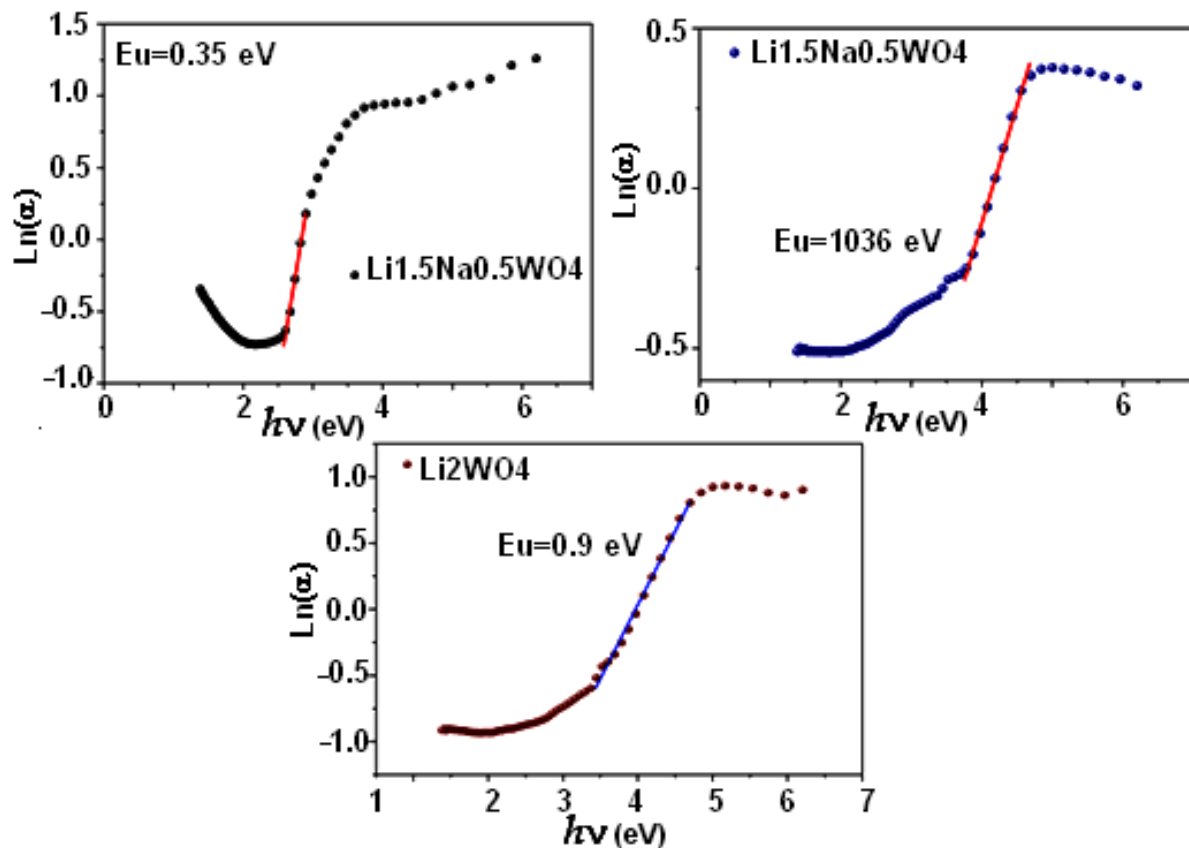


Figure 5. Urbach energy for the three compounds.

Table 2. Densities of localized states and the values of Urbach energy for the studied compounds.

Sample	$\text{Li}_{0.5}\text{Na}_{1.5}\text{WO}_4$	$\text{Li}_{1.5}\text{Na}_{0.5}\text{WO}_4$	$\text{Li}_2\text{WO}_4$
Density of localized states	$0.6 \times 10^{20}$ – $6 \times 10^{20}$	$1.10^{22}$ – $2.10^{24}$	$1.10^{22}$ – $9.10^{23}$
Value of Urbach energy	0.35 (eV)	1.36 (eV)	0.9 (eV)

### 3.3. Thermal Analysis

A differential scanning calorimetric analysis is commonly used to analyze a material's thermal change, such as melting, glass transition, crystallization, and so on. Therefore, to avoid reactivity with the atmosphere, this analysis was carried out in the presence of an argon atmosphere. The thermal investigations were carried out in a temperature range of ambient temperature to 450 K with a scan rate of 5  $^{\circ}\text{C}/\text{min}$ . The obtained thermograms are shown in Figure 6. As shown, the compound  $\text{Li}_{1.5}\text{Na}_{0.5}\text{WO}_4$  has three endothermic peaks, at  $T = 365$  K,  $T = 379$  K, and  $T = 397$  K (Figure 6a) [6], whereas  $\text{Li}_{0.5}\text{Na}_{1.5}\text{WO}_4$  has just two endothermic peaks, at  $T = 379$  K and  $T = 397$  K (Figure 6b) [35].

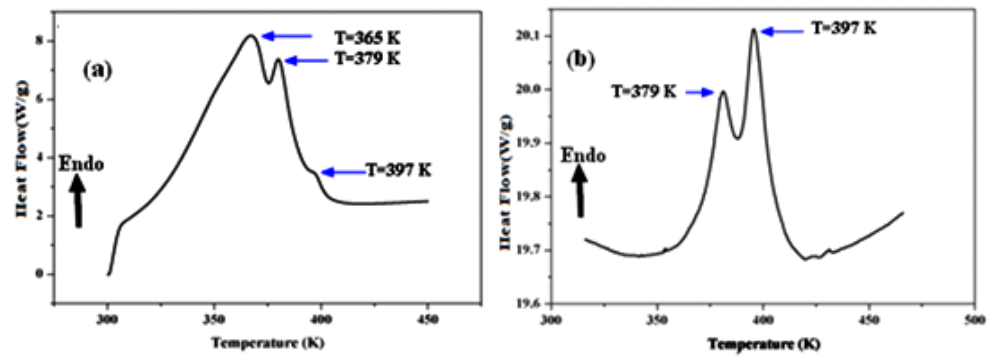


Figure 6. Differential scanning calorimetric of (a)  $\text{Li}_{1.5}\text{Na}_{0.5}\text{WO}_4$  and (b)  $\text{Li}_{0.5}\text{Na}_{1.5}\text{WO}_4$  [36,38].

The thermal examination of the parent compounds  $\text{Li}_2\text{WO}_4$  and  $\text{Na}_2\text{WO}_4$  revealed the presence of a peak at 373 K, which was attributed to the ferroelectric/paraelectric transition and confirmed by the dielectric research [5,6]. The broad peak at 365 K may be due to the progressive release of  $\text{H}_2\text{O}$  absorbed by the material at ambient temperature, which shows that this material has a hygroscopic character. Based on Ref. [6] and the impact of the composition difference, we can credit the peak found at  $T = 397$  K for both compounds to the ferroelectric–paraelectric transition. In addition, to verify this result we investigated the dielectric characteristics of the compounds  $\text{Li}_{1.5}\text{Na}_{0.5}\text{WO}_4$  and  $\text{Li}_{0.5}\text{Na}_{1.5}\text{WO}_4$ .

### 3.4. Dielectric Studies

Figures 7 and 8 show the temperature dependency of the dielectric constant for the compounds  $\text{Li}_{0.5}\text{Na}_{1.5}\text{WO}_4$  and  $\text{Li}_{1.5}\text{Na}_{0.5}\text{WO}_4$ . The study of dielectric characteristics is, therefore, essential in order to detect the changes in the phases, the properties, and the behavior of the examined substance when an electric field is applied. This investigation is undertaken in the present case as a function of temperature in the range of 300–650 K, and in a frequency range of 100 Hz to 1 MHz. In fact, Figures 7a,b and 8a,b show the temperature dependence of the relative dielectric constant with a fixed frequency for the compounds  $\text{Li}_{0.5}\text{Na}_{1.5}\text{WO}_4$  and  $\text{Li}_{1.5}\text{Na}_{0.5}\text{WO}_4$  [34], respectively.

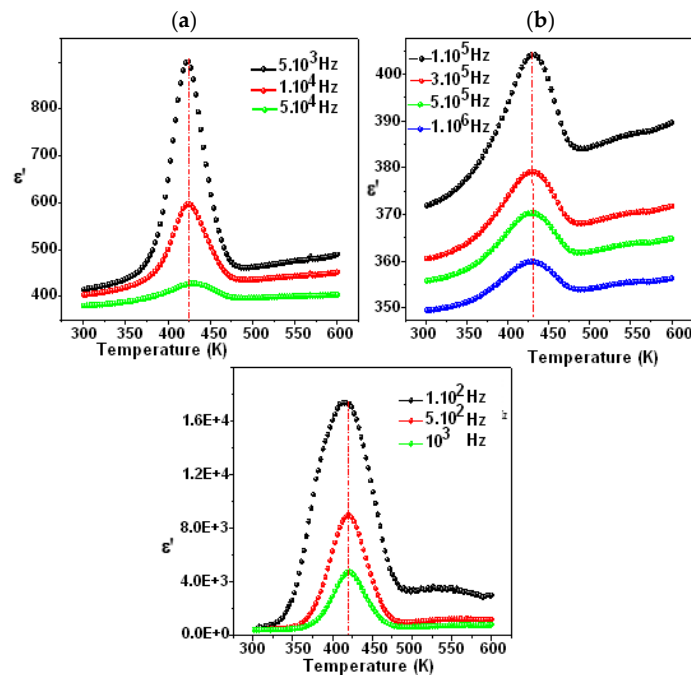
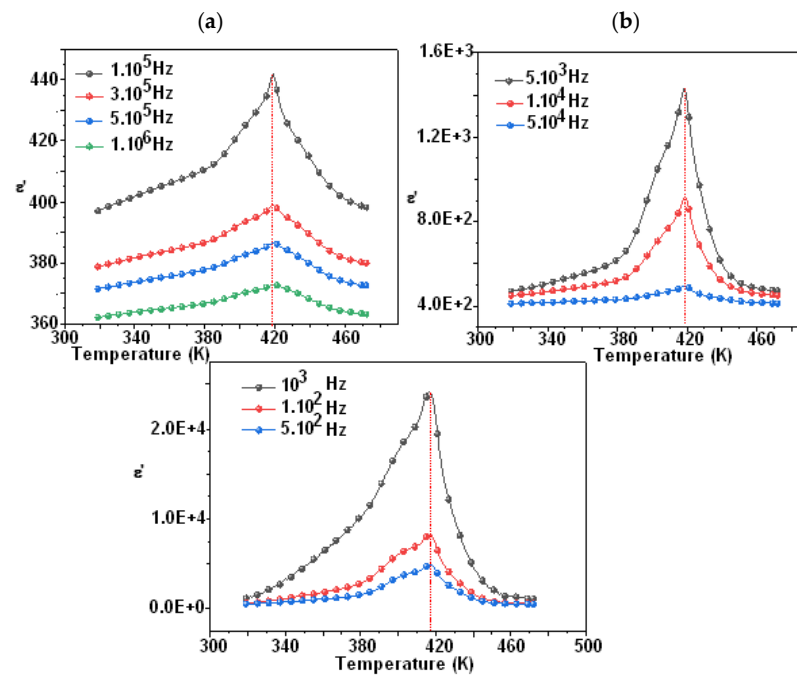


Figure 7. Variation in  $\epsilon'$  as a function of temperature for  $\text{Li}_{1.5}\text{Na}_{0.5}\text{WO}_4$  ((a) frequency from 100 Hz to 10,000 Hz and (b) frequency from 100,000 to 1,000,000 Hz) [36].



**Figure 8.** Variation in  $\epsilon'$  as function temperature of  $\text{Li}_{0.5}\text{Na}_{1.5}\text{WO}_4$  ((a) frequency from 100 Hz to 10,000 Hz and (b) frequency from 100,000 to 1,000,000 Hz).

We can see a dielectric relaxation of about 421 K for the compound  $\text{Li}_{1.5}\text{Na}_{0.5}\text{WO}_4$  and 418 K for the compound  $\text{Li}_{1.5}\text{Na}_{0.5}\text{WO}_4$ . Therefore, a para-ferroelectric phase transition may be related to this large dielectric peak at  $T_c$ . Its maximum does not change ( $T_c$  remains constant at different frequencies), but its magnitude diminishes as the frequency increases. This relaxation is also observed for the parent molecule at about 373 K [5,6]. This shift in transition temperature could be attributed to a change in symmetry caused by the composition change. Actually, a qualitative study of these curves revealed that  $T_c$  remained constant when the frequency was varied, confirming the examined compound's traditional characteristic [48]. Hence, in order to verify the nature of classic or relaxer ferroelectrics, Uchino and Nomura [49] proposed a more general expression of the Curie–Weiss law by introducing the degree of relaxation  $\gamma$ :

$$\frac{1}{\epsilon'} - \frac{1}{\epsilon'_{max}} = \frac{(T - T_c)^\gamma}{C} \quad (6)$$

where  $C$  is the Curie–Weiss constant,  $\epsilon'_{max}$  is the real dielectric constant at  $T = T_c$ , and  $\gamma$  ( $1 < \gamma < 2$ ) denotes the degree of relaxation. The diffuse nature of the transition is translated by the component  $\gamma$ . However, the  $\gamma$  value is close to 1 for classical ferroelectrics and should equal 2 for perfect relaxer ferroelectrics [50,51].

Figures 9 and 10 illustrate the logarithmic charts of Equation (5) at various frequencies (the curve fitted to the modified Curie–Weiss law is indicated by the solid red lines).

The obtained values for the  $\text{Li}_{1.5}\text{Na}_{0.5}\text{WO}_4$  and  $\text{Li}_{0.5}\text{Na}_{1.5}\text{WO}_4$  compounds are around 1.3 [34] and 1.5, respectively. This finding demonstrates that our sample is a typical ferroelectric compound. The dielectric measurements in the paraelectric state match the Curie–Weiss law rather well, as stated by the following relation:

$$\epsilon' = \frac{C}{T - T_0} \quad (7)$$

where  $C$  and  $T_0$  are the Curie–Weiss constant and temperature, respectively.

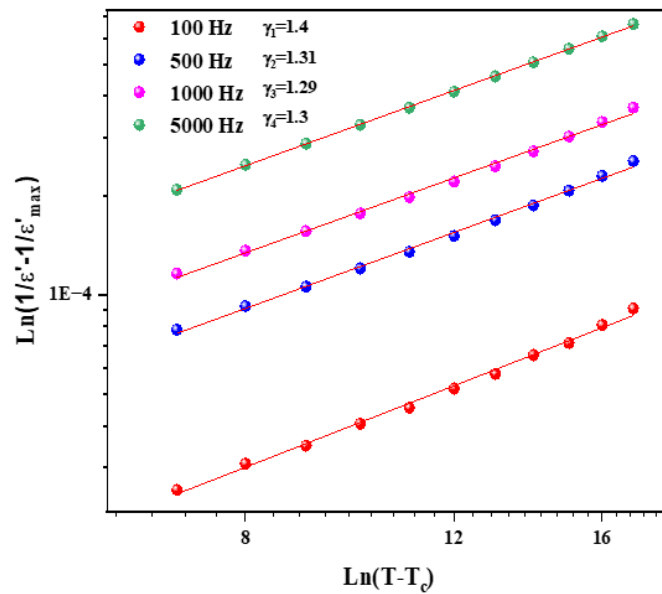


Figure 9.  $\ln\left(\frac{1}{\epsilon'} - \frac{1}{\epsilon'_{max}}\right)$  as function of  $\ln(T - T_c)$  for different frequencies for  $\text{Li}_{1.5}\text{Na}_{0.5}\text{WO}_4$  compound.

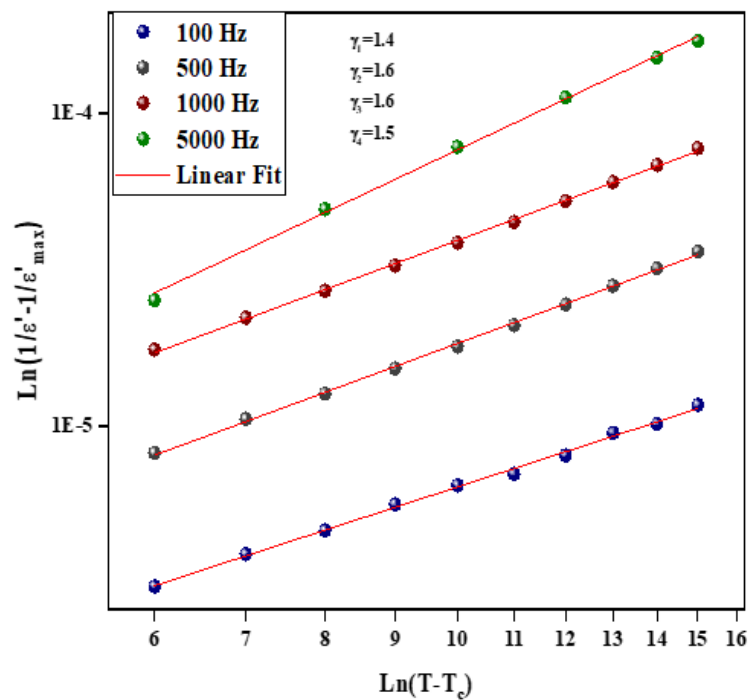


Figure 10.  $\ln\left(\frac{1}{\epsilon'} - \frac{1}{\epsilon'_{max}}\right)$  as function of  $\ln(T - T_c)$  for different frequency for  $\text{Li}_{0.5}\text{Na}_{1.5}\text{WO}_4$  compound.

Figure 11 depicts the temperature dependency of the dielectric reciprocal ( $1/\epsilon'$ ) at 500 Hz. Indeed, for  $\text{Li}_{0.5}\text{Na}_{1.5}\text{WO}_4$  and  $\text{Li}_{1.5}\text{Na}_{0.5}\text{WO}_4$ , these plots display straight lines, with the  $x$ -axis intercepts at  $T_0 = 418$  K and  $421$  K [34]. In classical ferroelectrics, the value of  $T_0$  indicates the order of the para-ferroelectric phase transition. In the case of  $T_0 \neq T_C$ , the phase transition is first order. If  $T_0 = T_C$ , then this transition is of second order [52]. According to our observations, the value of  $T_0$  is comparable to  $T_C$ , suggesting that this transition is of second order [53]. Beginning with the concept of  $\epsilon'$ , which is connected to capacitance and the alignment of the dipole that is observed, we may deduce that a rise in frequency corresponds to an increase in disorder, which causes  $\epsilon'$  to drop. It is evident from comparing the  $\epsilon'$  values of the studied compounds that  $\text{Li}_{0.5}\text{Na}_{1.5}\text{WO}_4$  has higher values than  $\text{Li}_{1.5}\text{Na}_{0.5}\text{WO}_4$ . We could, therefore, conclude that the latter is the most disordered.

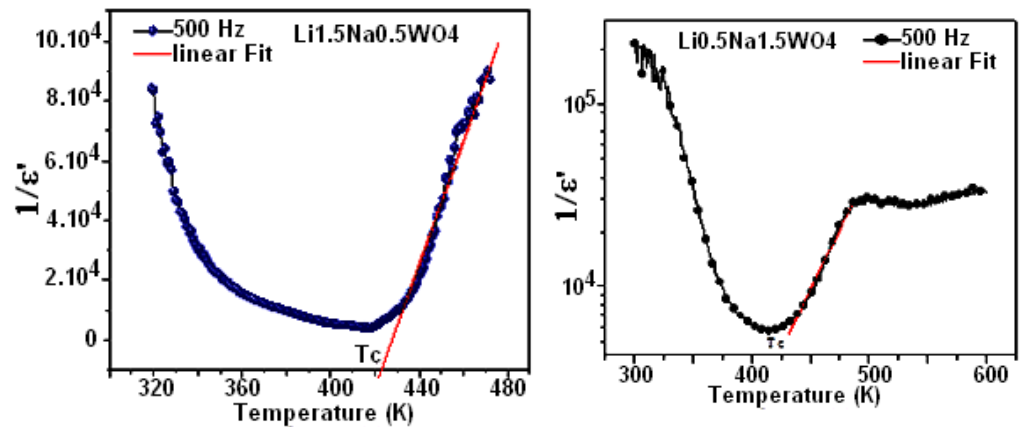


Figure 11. Temperature variation in  $(1/\epsilon')$  at 500 Hz.

### 3.5. Conductivity Analysis

For the three compounds under investigation, we have calculated the conductivity fluctuation as a function of the frequency of the various temperature values [6,34,35]. We also observed that the experimental variation in conductivity is described by Jonscher’s universal law. The experimental results were adopted using the equation

$$\sigma_{AC}(W) = \sigma_{DC} + A\omega^S \tag{8}$$

In fact, as shown in Figure 12, and based on this adjustment, we have plotted the curves  $\text{Ln}(\sigma_{DC}) = f\left(\frac{1000}{T}\right)$  which are adjusted by the following expression:

$$\sigma_{DC} = \sigma_0 \exp\left(\frac{-E_a}{K_B T}\right) \tag{9}$$

where  $\sigma_0$  is the pre-exponential factor given by the following expression:

$$\sigma_0 = \left(\frac{e_a^2 a_h^2 \gamma_0}{6k}\right) N(T) \exp\left(\frac{S_\mu}{k}\right) \tag{10}$$

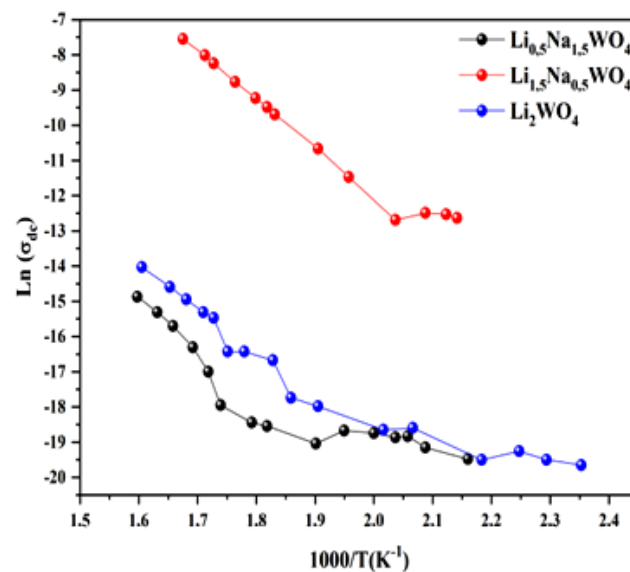


Figure 12. Variation in conductivity for the three studied compounds.

The number of charge carriers that contribute to the conduction  $N$  and the entropy  $S$  are both proportional to this factor. Since the activation energies of the three materials are of the same order of magnitude, the high conductivity of the  $\text{Li}_{1.5}\text{Na}_{0.5}\text{WO}_4$  combination can be explained by other factors (Table 2). Moreover, given that the number of charge carriers is related to the density of the localized states ( $N = kTN(EF)$ ) [54], the number in  $\text{Li}_{1.5}\text{Na}_{0.5}\text{WO}_4$  is greater than those in  $\text{Li}_2\text{WO}_4$  and  $\text{Li}_{0.5}\text{Na}_{1.5}\text{WO}_4$ . The enormous value of the Urbach energy for the composite  $\text{Li}_{1.5}\text{Na}_{0.5}\text{WO}_4$  compared to the other two compounds indicates that the disorder (translated by the entropy  $S$ ) in this material is more important, and thus:  $S(x = 0.5) > S(x = 1) > S(x = 1.5)$ . Actually, a comparative study revealed that the conductivity of the compound  $\text{Li}_{1.5}\text{Na}_{0.5}\text{WO}_4$  is greater than that of the other two compounds, which can be explained by the fact that the disorder (entropy represented by the Urbach energy) and the number of charge carriers (represented by the number of localized states) is greater for this compound than for the other two.

#### 4. Conclusions

The obtained results allow us to deduce that the compounds  $\text{Li}_2\text{WO}_4$  and  $\text{Li}_{1.5}\text{Na}_{0.5}\text{WO}_4$  crystallize in the monoclinic system while the compound  $\text{Li}_{0.5}\text{Na}_{1.5}\text{WO}_4$  crystallizes in the orthorhombic system. The values obtained from the estimation of the crystallite sizes of these compounds range between 0.2 and 0.1  $\mu\text{m}$ , which is smaller than the grain sizes that were determined from the SEM images, which range from 3 to 5  $\mu\text{m}$ . The SEM images clearly show that the compounds' structures are compact, with a small number of pores resulting from the compounds' tendency to form agglomerations. The EDX analysis verifies that the chemical elements are present in the compositions of the samples. Additionally, we can state that the optical analysis carried out with a UV-Vis spectrophotometer showed that the two compounds  $\text{Li}_{1.5}\text{Na}_{0.5}\text{WO}_4$  and  $\text{Li}_2\text{WO}_4$  each had a single absorption band present at 245 nm, while  $\text{Li}_{0.5}\text{Na}_{1.5}\text{WO}_4$  had a single absorption band at 300 nm. In fact, this difference could be explained by the shift in symmetry from orthorhombic to monoclinic. Then, the optical gap energy was calculated using the Kubelka–Munk equation. In addition, the Urbach energy calculation revealed that the compound  $\text{Li}_{1.5}\text{Na}_{0.5}\text{WO}_4$  is the most disordered of the three investigated. The dielectric studies of the two compounds also revealed the presence of ferro–paraelectric transitions at 421 K and 418 K for  $\text{Li}_{0.5}\text{Na}_{1.5}\text{WO}_4$  and  $\text{Li}_{1.5}\text{Na}_{0.5}\text{WO}_4$ . Thermal research detected this transition (DSC), which occurs in the parent compounds at about 373 K; where the temperature offset may be due to symmetry differences. Moreover, a comparison study revealed that the conductivity of the compound  $\text{Li}_{1.5}\text{Na}_{0.5}\text{WO}_4$  is greater than that of the other two compounds, which may be due to the fact that the disorder and the charge number are higher in the case of  $\text{Li}_{1.5}\text{Na}_{0.5}\text{WO}_4$ .

**Author Contributions:** Conceptualization, M.K. (Moufida Krimi) and A.B.R.; methodology, K.K.; software, M.K. (Moufida Krimi) and M.H.A.-H.; validation, M.K., A.B.R. and A.H.A.; formal analysis, M.K. (Moufida Krimi); investigation, A.B.R.; data curation, K.K.; writing—original draft preparation, M.K. (Moufida Krimi) and A.B.R.; writing—review and editing, A.B.R., M.K. (Mohamed Khitouni) and K.K.; supervision, A.B.R. All authors have read and agreed to the published version of the manuscript.

**Funding:** This research received no external funding.

**Data Availability Statement:** Data can be requested from the authors.

**Acknowledgments:** Researchers would like to thank the Deanship of Scientific Research, Qassim University for the funding publication of this project.

**Conflicts of Interest:** The authors declare no conflict of interest.

## References

1. Deb, K.K. Pyroelectric characteristics of  $(\text{Pb}_{0.9}\text{Sm}_{0.1})\text{TiO}_3$  ceramics. *Ferroelectrics* **1988**, *82*, 45–53. [[CrossRef](#)]
2. Tandon, R.P.; Singh, R.; Singh, V.; Swani, N.H.; Hans, V.K. Ferroelectric properties of lead titanate/polymer composite and its application in hydrophones. *J. Mater. Sci. Lett.* **1992**, *11*, 883–885. [[CrossRef](#)]
3. Alvarez-Vega, M.; Rodriguez-Carvajal, J.; Reyes-Cardenas, J.G.; Fuentes, A.F.; Amador, U. A Topological Analysis of Void Spaces in Tungstate Frameworks: Assessing Storage Properties for the Environmentally Important Guest Molecules and Ions:  $\text{CO}_2$ ,  $\text{UO}_2$ ,  $\text{PuO}_2$ , U, Pu,  $\text{Sr}^{2+}$ ,  $\text{Cs}^+$ ,  $\text{CH}_4$ , and  $\text{H}_2$ . *J. Chem. Mater.* **2001**, *13*, 3871–3875.
4. Wong, C.P.P.; Lai, C.W.; Lee, K.M. Tungsten-Based Materials for Supercapacitors. In *Book Inorganic Nanomaterials for Supercapacitor Design*, 1st ed.; CRC Press: Boca Raton, FL, USA, 2020; Volume 11. [[CrossRef](#)]
5. Isupov, V.A. Ferroelectric and Ferroelastic Phase Transitions in Molybdates and Tungstates of Monovalent and Bivalent Elements. *Ferroelectrics* **2005**, *322*, 83–114. [[CrossRef](#)]
6. Sharma, S.; Choudhary, R.N.P. Phase transition in  $\text{Li}_2\text{WO}_4$ . *Ferroelectrics* **1999**, *4*, 129–137. [[CrossRef](#)]
7. Besozzi, E.; Dellasega, D.; Pezzoli, A.; Conti, C.; Passoni, M.; Beghi, M.G. Amorphous, ultra-nano- and nano-crystalline tungsten-based coatings grown by Pulsed Laser Deposition: Mechanical characterization by Surface Brillouin Spectroscopy. *Mater. Des.* **2016**, *106*, 14–21. [[CrossRef](#)]
8. Sharma, S.; Choudhary, R.N.P.; Shanigrahi, S.R. Structural and electrical properties of  $\text{Na}_2\text{WO}_4$  ceramics. *J. Mater. Lett.* **1999**, *40*, 134–139. [[CrossRef](#)]
9. Bazarova, Z.G.; Arkhincheyeva, S.I.; Batuyeva, I.S.; Bazarov, B.G.; Tushinova, Y.I.; Bazarova, S.T.; Fyodorov, K.N. Complex Oxide Compounds of Polyvalent Metals: Synthesis, Structure and Properties. *Chem. Sustain. Dev.* **2000**, *8*, 135–139.
10. Nagasaki, T.; Kok, K.; Yahaya, A.H.; Igawa, N.; Noda, K.; Ohno, H. Phase identification and electrical conductivity of  $\text{Li}_2\text{WO}_4$  Reviewed. *Solid State Ion.* **1997**, *96*, 61–74. [[CrossRef](#)]
11. Busey, R.H.; Keller, O.L., Jr. Structure of the Aqueous Pertechetate Ion by Raman and Infrared Spectroscopy. Raman and Infrared Spectra of Crystalline  $\text{KTCO}_4$ ,  $\text{KReO}_4$ ,  $\text{Na}_2\text{MoO}_4$ ,  $\text{Na}_2\text{WO}_4$ ,  $\text{Na}_2\text{MoO}_4 \cdot 2\text{H}_2\text{O}$ , and  $\text{Na}_2\text{WO}_4 \cdot 2\text{H}_2\text{O}$ . *J. Chem. Phys.* **1964**, *41*, 215–225. [[CrossRef](#)]
12. Pal, I.; Agarwal, A.; Sanghi, S.; Shearan, A.; Ahlawat, N. Conductivity and dielectric relaxation in sodium borosulfate glasses. *J. Alloys Compd.* **2009**, *472*, 40–45. [[CrossRef](#)]
13. Dyre, J.C. The random free-energy barrier model for ac conduction in disordered solids. *J. Appl. Phys.* **1988**, *64*, 2456–2468. [[CrossRef](#)]
14. Karoui, K.; Rhaiem, A.B.; Jomni, F.; Moneger, J.L.; Bulou, A.; Guidara, K. Characterization of phase transitions of  $[\text{N}(\text{CH}_3)_4]_2\text{ZnCl}_2\text{Br}_2$  mixed crystals. *J. Mol. Struct.* **2013**, *1048*, 287–294. [[CrossRef](#)]
15. Huebner, J.S.; Dillenburg, R.G. Impedance spectra of hot, dry silicate minerals and rock: Qualitative interpretation of spectra. *J. Am. Mineral.* **1995**, *80*, 46–64. [[CrossRef](#)]
16. Imran, M.M.A.; Lafi, O.A. Electrical conductivity, density of states and optical band gap in  $\text{Se}_{90}\text{Te}_6\text{Sn}_4$  glassy semiconductor. *Physica B* **2013**, *410*, 201–205. [[CrossRef](#)]
17. Bhowmik, R.N.; Vijayasri, G. Study of microstructure and semiconductor to metallic conductivity transition in solid state sintered  $\text{Li}_{0.5}\text{Mn}_{0.5}\text{Fe}_2\text{O}_4 - \delta$  spinel ferrite. *J. Appl. Phys.* **2013**, *114*, 223701. [[CrossRef](#)]
18. Bhowmik, R.N.; Aneesh Kumar, K.S. Role of pH value during material synthesis and grain-grain boundary contribution on the observed semiconductor to metal like conductivity transition in  $\text{Ni}_{1.5}\text{Fe}_{1.5}\text{O}_4$  spinel ferrite. *Mater. Chem. Phys.* **2016**, *177*, 417–428. [[CrossRef](#)]
19. Saraswat, V.K.; Singh, K.; Saxena, N.S.; Kishore, V.; Sharma, T.P.; Saraswat, P.K. Composition dependence of the electrical conductivity of  $\text{Se}_{85-x}\text{Te}_{15}\text{Sb}_x$  ( $x = 2, 4, 6, 8$  and  $10$ ) glass at room temperature. *Curr. Appl. Phys.* **2006**, *6*, 14–18. [[CrossRef](#)]
20. Pradhan, S.K.; Kalidoss, J.; Barik, R.; Sivaiah, B.; Dhar, A.; Bajpai, S. Development of high density tungsten based scandate by Spark Plasma Sintering for the application in microwave tube devices. *Int. J. Refract. Metals Hard Mater.* **2016**, *61*, 215–224. [[CrossRef](#)]
21. Namikawa, H. Characterization of the diffusion process in oxide glasses based on the correlation between electric conduction and dielectric relaxation. *J. Non-Cryst. Solids* **1975**, *18*, 173–195. [[CrossRef](#)]
22. Gudmundsson, J.T.; Svavarsson, H.G.; Gudjonsson, S.; Gislason, H.P. Frequency-dependent conductivity in lithium-diffused and annealed GaAs. *Phys. B Condens. Matter* **2003**, *340–342*, 324–328. [[CrossRef](#)]
23. van den Berg, A.J.; Tuinstra, F.; Warczewski, J. Modulated structures of some alkali molybdates and tungstates. *Acta Cryst. B* **1973**, *29*, 586–589. [[CrossRef](#)]
24. Mollah, S.; Som, K.K.; Chaudri, K.B. AC conductivity in  $\text{Bi}_4\text{Sr}_3\text{Ca}_3\text{Cu}_y\text{O}_x$  ( $y=0-5$ ) and  $\text{Bi}_4\text{Sr}_3\text{Ca}_{3-z}\text{Li}_z\text{Cu}_4\text{O}_x$  ( $z=0.1-1.0$ ) semiconducting oxide glasses. *J. Appl. Phys.* **1993**, *74*, 931–937. [[CrossRef](#)]
25. Hayashi, T.; Okada, J.; Toda, E.; Kuzuo, R.; Matsuda, Y.; Kuwata, N.; Kawamura, J. Electrochemical effect of lithium tungsten oxide modification on  $\text{LiCoO}_2$  thin film electrode. *J. Power Sources* **2015**, *285*, 559–567. [[CrossRef](#)]
26. Radzikhovskaya, M.A.; Garkushin, I.K.; Danilushikina, E.G. Ternary systems  $\text{LiBr-Li}_2\text{MoO}_4\text{-Li}_2\text{WO}_4$  and  $\text{LiF-Li}_2\text{MoO}_4\text{-Li}_2\text{WO}_4$ . *Russ. J. Inorg Chem.* **2012**, *57*, 1616–1620. [[CrossRef](#)]
27. Barinova, O.; Sadvoskiy, A.; Ermochenkov, I.; Kirsanova, S.; Khomyakov, A.; Zykova, M.; Kuchuk, Z.; Avetissov, I. Solid solution  $\text{Li}_2\text{MoO}_4 - \text{Li}_2\text{WO}_4$  crystal growth and characterization. *Cryst. Growth* **2017**, *468*, 365–368. [[CrossRef](#)]

28. Dkhilalli, F.; Megdiche, S.; Guidara, K.; Rasheed, M.; Barillé, R.; Megdiche, M. AC conductivity evolution in bulk and grain boundary response of sodium tungstate  $\text{Na}_2\text{WO}_4$ . *Ionics* **2017**, *24*, 169–180. [[CrossRef](#)]
29. Johan, M.R.; Han, T.K.; Arof, A.K. Growth and sintering effects of hydrated polycrystalline  $\text{Li}_2\text{WO}_4$ . *Ionics* **2010**, *16*, 323–333. [[CrossRef](#)]
30. Luz Lima, C.; Saraiva, G.D.; Freire, P.T.C.; Maczka, M.; Paraguassu, W.; de Sousa, F.F.; Filho, J.M. Temperature-induced phase transformations in  $\text{Na}_2\text{WO}_4$  and  $\text{Na}_2\text{MoO}_4$  crystals. *Raman Spectrosc.* **2011**, *42*, 799–802. [[CrossRef](#)]
31. Zhou, D.; Randall, C.A.; Pang, L.-X.; Wang, H.; Guo, J.; Zhang, G.-Q.; Wu, X.-G.; Shui, L.; Yao, X. Microwave Dielectric Properties of  $\text{Li}_2\text{WO}_4$  Ceramic with Ultra-Low Sintering Temperature. *J. Am. Ceram. Soc.* **2011**, *94*, 348–350. [[CrossRef](#)]
32. Bárbara, F.; Joséa, E. Antiferromagnetic and Ferroelectric Phase Transitions and Instabilities in PFW-PT Multiferroic Solid Solution Characterized by Anelastic Measurement. *Ferroelectrics* **2013**, *448*, 86–95.
33. Urusova, M.A.; Valyashko, V.M. High-temperature equilibria and critical phenomena in the  $\text{Na}_2\text{CO}_3$ - $\text{NaCl}$ - $\text{H}_2\text{O}$  and  $\text{Na}_2\text{CO}_3$ - $\text{Na}_2\text{WO}_4$ - $\text{H}_2\text{O}$  systems. *Russ. J. Inorg. Chem.* **2011**, *56*, 430–441. [[CrossRef](#)]
34. Krimi, M.; Karoui, K.; Sunol, J.J.; Rhaïem, A.B. Phase transition, impedance spectroscopy and conduction mechanism of  $\text{Li}_{0.5}\text{Na}_{1.5}\text{WO}_4$  material. *Phys. E Low-Dimens. Syst. Nanostruct.* **2018**, *102*, 137–145. [[CrossRef](#)]
35. Krimi, M.; Karoui, K.; Suñol, J.J.; Rhaïem, A.B. Optical and electrical properties of  $\text{Li}_2\text{WO}_4$  compound. *Phase Trans.* **2019**, *92*, 737–754. [[CrossRef](#)]
36. Mallah, A.; Al-Thuwayb, F.; Khitouni, M.; Alsawi, A.; Suñol, J.J.; Greneche, J.-M.; Almoneef, M.M. Synthesis, Structural and Magnetic Characterization of Superparamagnetic  $\text{Ni}_{0.3}\text{Zn}_{0.7}\text{Cr}_{2-x}\text{Fe}_x\text{O}_4$  Oxides Obtained by Sol-Gel Method. *Crystals* **2023**, *13*, 894. [[CrossRef](#)]
37. Warren, B.E. *X-ray Diffraction*; Dover: New York, NY, USA, 1990; pp. 251–275.
38. Williamson, G.K.; Hall, W.H. X-ray line broadening from filed aluminium and wolfram. *Acta Metall.* **1953**, *1*, 22–31. [[CrossRef](#)]
39. Kuschke, W.M.; Keller, R.M.; Grahle, P.; Mason, R.; Arzt, E. Mechanisms of Powder Milling Investigated by X-ray Diffraction and Quantitative Metallography. *Z. Metallkd.* **1995**, *86*, 804–813. [[CrossRef](#)]
40. Aleksandrov, I.V.; Valiev, R.Z. Studies of Nanocrystalline Materials by X-ray Diffraction Techniques. *Phys. Met. Metallogr.* **1994**, *77*, 623–629.
41. Halder, N.C.; Wagner, C.N. Analysis of the Broadening of Powder Pattern Peaks Using Variance, Integral Breadth, and Fourier Coefficients of the Line Profile. *Adv. X-ray Anal.* **1966**, *9*, 91–102.
42. Daly, R.; Khitouni, M.; Kolsi, A.W.; Njah, N. The studies of crystallite size and microstrains in aluminum powder prepared by mechanical milling. *Phys. Stat. Solidi C* **2006**, *3*, 3325–3331. [[CrossRef](#)]
43. Khitouni, M.; Kolsi, A.W.; Njah, N. The effects of boron additions on the disordering and crystallite refinement of  $\text{Ni}_3\text{Al}$  powders during mechanical milling. *Ann. Chim. Sci. Matériaux* **2003**, *28*, 17–29. [[CrossRef](#)]
44. Barhoumi, A.; Leroy, G.; Duponchel, B.; Gest, J.; Yang, L.; Waldhoff, N.; Guermazi, S. Aluminum doped ZnO thin films deposited by direct current sputtering: Structural and optical properties. *Superlattices Microstruct.* **2015**, *82*, 483–498. [[CrossRef](#)]
45. Kubelka, P.; Munk, F. An article on optics of paint layers. *Z. Tech. Phys.* **1931**, *12*, 259–274.
46. Bougrine, A.; El Hichou, A.; Addou, M.; Ebothé, J.; Kachouane, A.; Troyon, M. Structural, optical and cathodoluminescence characteristics of undoped and tin-doped ZnO thin films prepared by spray pyrolysis. *J. Mater. Chem. Phys.* **2003**, *80*, 438–445. [[CrossRef](#)]
47. Enneffati, M.; Maaloul, N.K.; Louati, B.; Guidara, K. Synthesis, vibrational and UV-visible studies of sodium cadmium orthophosphate. *Opt. Quantum Electron.* **2017**, *49*, 331. [[CrossRef](#)]
48. Ben Nasr, W.; Karoui, K.; Bulou, A.; Ben Rhaïem, A.  $\text{Li}_{1.5}\text{Rb}_{0.5}\text{MoO}_4$ : Ferroelectric properties and characterization of phase transitions by Raman spectroscopy. *Phys. E Low-Dimens. Syst. Nanostruct.* **2017**, *93*, 339–344. [[CrossRef](#)]
49. Uchino, K.; Nomura, S. Critical Exponents of the Dielectric Constants in Diffused-Phase-Transition Crystals. *Ferroelectr. Lett. Sect.* **1982**, *44*, 55–61. [[CrossRef](#)]
50. Viehland, D.; Wuttig, M.; Cross, L.E. The glassy behavior of relaxor ferroelectrics. *Ferroelectrics* **2011**, *120*, 71–77. [[CrossRef](#)]
51. Tan, Y.-Q.; Yuan, Y.; Hao, Y.-M.; Dong, S.-Y.; Yang, Y.-W. Structure and dielectric properties of  $\text{Ba}_5\text{NdCu}_{1.5}\text{Nb}_{8.5}\text{O}_{30-\delta}$  tungsten bronze ceramics. *Mater. Res. Bull.* **2013**, *48*, 1934–1938. [[CrossRef](#)]
52. Rhaïem, A.; Jomni, F.; Karoui, K.; Guidara, K. Ferroelectric properties of the  $[\text{N}(\text{CH}_3)_4]_2\text{CoCl}_2\text{Br}_2$  compound. *J. Mol. Struct.* **2013**, *1035*, 140–144. [[CrossRef](#)]
53. Hajji, R.; Oueslati, A.; Hajlaoui, F.; Bulou, A.; Hlel, F. Structural characterization, thermal, ac conductivity and dielectric properties of  $(\text{C}_7\text{H}_{12}\text{N}_2)_2[\text{SnCl}_6]\text{Cl}_2 \cdot 1.5\text{H}_2\text{O}$ . *Phase Trans.* **2016**, *89*, 523–542. [[CrossRef](#)]
54. Long, A.R. Frequency-Dependent Loss in Amorphous Semiconductors. *J. Adv. Phys.* **1982**, *31*, 553–637. [[CrossRef](#)]

**Disclaimer/Publisher’s Note:** The statements, opinions and data contained in all publications are solely those of the individual author(s) and contributor(s) and not of MDPI and/or the editor(s). MDPI and/or the editor(s) disclaim responsibility for any injury to people or property resulting from any ideas, methods, instructions or products referred to in the content.